Sensorless Adaptive and Predictive Control of PMSM Based on FOC Strategy

Marcel Nicola* and Claudiu-Ionel Nicola*,†
* National Institute for Research, Development and Testing in Electrical Engineering – ICMET / Research Department, Craiova, Romania, marcel_nicola@yahoo.com
† University of Craiova / Department of Automatic Control and Electronics, Craiova, Romania, claudiu@automation.ucv.ro

***Abstract* - This article presents a sensorless control structure for a PMSM (Permanent Magnet Synchronous Motor), with a MRAC (Model Reference Adaptive Controller) type speed controller, FOC (Field Oriented Control) type overall control strategy, and d-q axis type reference system, for which the I_d current reference set to zero is selected for reasons of torque maximization, and the current reference is supplied by the MRAC adaptive controller output. The numerical simulations results obtained in the case of parameter variation and rapidly varying load torque with a random component, plus an adjustment mechanism described by first-order differential equations recommend the implementation of this structure in an embedded system in real time. Also, presents a sensorless MPC (Model Predictive Control) for a PMSM in which the rotor speed is provided by a MRAS (Model Reference Adaptive System) observer. The results of the numerical simulations show the superiority of the MPC control system compared to FOC type control system in the case of parameter variation and rapidly varying torque load with a random component. The relatively low complexity of the number of arithmetic operations required to implement the estimation and control algorithms recommends the implementation of an embedded system in real time in future works.**

Cuvinte cheie: *PMSM, FOC, control adaptiv, control predictiv, observer de stare.*

Keywords: *PMSM, FOC, adaptive control, predictive control, state observer.*

I. INTRODUCTION

In the last decade, a significant increase is noticed in the use of PMSM's in electric drives with applications in robotics, electrical vehicles, machine tools, peripherals equipment for computers, etc. This increased interest for PMSM's is due to certain advantages over other types of motors, such as: high duty density, small size, low-inertia, easier cooling and rapid torque response [1]. In addition, in [2] the high performance of PMSM control can be achieved due to the fact that the back-EMF is sinusoidal.

Among the standard PMSM control structures presented in [3-5] is mentioned DTC (Direct Torque Control) and FOC. In addition with these structures, a significant number of modern control methods have been inherently developed, such as: the robust control system [6], the model adaptive control [7-10], the model predictive control system [11-18], neuro-fuzzy control and intelligent control [19-22].

Among the modern PMSM control methods, the adaptive control methods hold a special place, considering that in the electric drive control a number of parameters vary with time, and the reference speed and the load torque can have very fast variations [7-10].

The results on the application of the predictive control of the induction motors are presented in [14] and in terms of motors with variable reluctance, a predictive speed loop controller is presented in [15]. The predictive control for the PMSM is presented in [16], but the results are presented for the current regulation loop without considering the external speed control loop and a global MPC of the currents and speed is presented in [17].

The type MPC systems have a special place among the control systems. They can be viewed as real-time optimization systems, and if their first industry applications were applied to relatively slow systems over the past decade, due to the significant increase in computing power in the embedded system with DSP, MPC application, the concern has expanded to fast systems over time. Some of the first works which deal with the application of the MPC strategy to electric drives, power convertors, and PMSMs are presented in [11-13].

To eliminate the speed sensors, which require additional costs and even the decrease in the reliability of the overall driving system, a series of speed observers have been developed for both induction motors in [23] and for PMSM's in [24-30].

Based on these aspects, this article presents an adaptive sensorless control structure for the speed control with FOC-type overall control strategy, where the current reference is selected for reasons of torque maximization, and the current reference is supplied by the MRAC adaptive controller output, and the speed is supplied by a back-EMF sliding mode observer. Also, presents a predictive control structure of currents for a PMSM where the global control structure is FOC type with a PI type external speed control that will generate a reference i_q^* for the predictive controller, and the reference $i_d^* = 0$ is chosen to maximize torque (I_d and I_q are stator currents in d-q axis frame).

The rest of paper is structured as follows: Section 2 describes the mathematical model of PMSM and adaptive control. The results of the numerical simulation for the classical FOC structure with PI controller versus MRAC controller are presented in Section 3. The hybrid model of PMSM and inverter is presented in Section 4. Section 5 presents the sensorless model of the predictive control using a MRAS observer. The results of the numerical simulation for the classical FOC structure with PI current controllers versus predictive current controller are presented in Section 6. In last section are presented some conclusions and ideas for future works.

II. PMSM And Adaptive Control – Mathematical Model

Following [8, 9], with the usual notation, in d-q model on rotor reference frame, the stator voltage equations are given by:

$$\begin{aligned} u_{qs} &= R_q i_{qs} + \rho\lambda_{ds} + \omega\lambda_{ds} \\ u_{ds} &= R_d i_{ds} + \rho\lambda_{ds} + \omega\lambda_{qs} \end{aligned} \tag{1}$$

where R_q, R_d and L_q, L_d are the quadrature and direct axis winding resistances and inductances of the PMSM drive and ρ is the the differential operator. The i_d, i_q and u_d, u_q are the d and q axes stator currents and voltages respectively. Note the rotor angular velocity with ω and the flux linkage ψ_f. For q and d axes the flux linkages are given by:

$$\begin{aligned} \lambda_{qs} &= L_q i_{qs} \\ \lambda_{ds} &= L_d i_{ds} + \psi_f \end{aligned} \tag{2}$$

By substituting equation (2) with (1) the result is:

$$\begin{bmatrix} u_{qs} \\ u_{ds} \end{bmatrix} = \begin{bmatrix} R_q & \omega L_d \\ -\omega L_q & R_q + \rho L_d \end{bmatrix} \begin{bmatrix} i_{qs} \\ i_{ds} \end{bmatrix} + \begin{bmatrix} \omega\psi_f \\ \rho\psi_f \end{bmatrix} \tag{3}$$

The electromagnetic torque (T_e) and the mechanical torque (T_m) developed in the PMSM drive are given by the equations:

$$\begin{aligned} T_e &= \frac{3}{2} n_p \left\{ \lambda_{ds} i_{qs} - \lambda_{qs} i_{ds} \right\} \\ T_m &= T_L + B\omega + J\frac{d\omega}{dt} \end{aligned} \tag{4}$$

where J represent the rotor inertia, B represent the viscous friction coefficient, n_p represent the pole pair number and T_L represent the load torque.

A reduced model of these equations, where L_d=L_q=L and R_s=R_q=R is presented in [9], in the following form:

$$\begin{pmatrix} \dot{i}_d \\ \dot{i}_q \\ \dot{\omega} \end{pmatrix} = \begin{pmatrix} -\dfrac{R_s}{L} & n_p\omega & 0 \\ -n_p\omega & -\dfrac{R_s}{L} & -\dfrac{n_p\psi_f}{L} \\ 0 & \dfrac{K_t}{J} & -\dfrac{B}{J} \end{pmatrix} \begin{pmatrix} i_d \\ i_q \\ \omega \end{pmatrix} + \begin{pmatrix} \dfrac{u_d}{L} \\ \dfrac{u_q}{L} \\ -\dfrac{T_L}{J} \end{pmatrix} \tag{5}$$

where K_t represent the torque constant.

Note $a = \dfrac{B}{J}$, $b = \dfrac{K_t}{J}$ and $d(t) = -\dfrac{T_L}{J} - \dfrac{K_t}{J}(i_q^* - i_q)$.

From (4) and (5) the speed equation is given by:

$$\dot{\omega} = -a\omega + b i_q^* + d(t) \tag{6}$$

The adaptive model is based on the FOC-type control strategy (see Fig. 1) with a cascade structure, with an outer speed control loop ω, and two inner control loops for i_d and i_q currents. The current reference $i_d^* = 0$ is selected in order to maximize the torque developed by the PMSM, and the i_q^* current reference is supplied by the MRAC adaptive controller output (see Fig. 2).

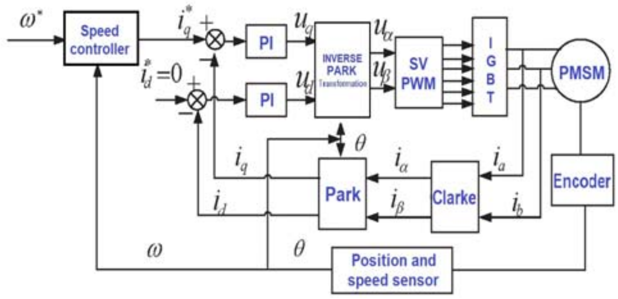

Fig. 1. FOC control strategy block diagram.

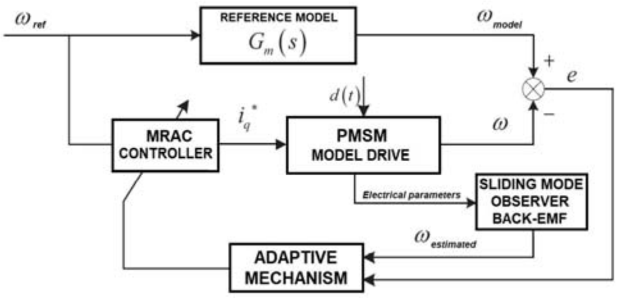

Fig. 2. MRAC block diagram.

For equation (6) of speed ω where the disturbance d(t) is negligible, the reference model in the following form is selected:

$$\dot{\omega}_m = -a_m\dot{\omega}_m + b_m\omega^* \tag{7}$$

where $a_m > 0$ and $b_m > 0$ are the parameters for this reference model.

Assuming the control law is described as:

$$i_q^* = h(t)\omega + l(t)\omega^* \tag{8}$$

where l(t) represent the variable feed-forward gain and h(t) represent the variable feedback gain.

Substituting (8) into (6), are obtained:

$$\dot{\omega} = -(a - bh(t))\omega + bl(t)\omega^* \tag{9}$$

The speed tracking error and the parameter error are defined as follows:

$$e = \omega_m - \omega \tag{10}$$

$$\phi = \begin{bmatrix} l^* - l(t) \\ h^* - h(t) \end{bmatrix} \tag{11}$$

where $l^* = \dfrac{b_m}{b}$ and $h^* = \dfrac{a - a_m}{b}$.

Then, differentiating (10) along system (7) and (9) are obtained:

$$\begin{aligned}\dot{e} &= -a_m\omega_m + b_m\omega^* + a\omega - bh(t)\omega - bl(t)\omega = \\ &= -a_m e + b\phi^T\left[\omega^* \quad \omega\right]^T\end{aligned} \tag{12}$$

Considering the Lyapunov function:

$$V = \frac{1}{2}e^2 + \frac{b}{2}\phi^T\begin{bmatrix}\gamma_1 & 0\\ 0 & \gamma_2\end{bmatrix}\phi \tag{13}$$

where $\gamma_1 > 0$ and $\gamma_2 > 0$.

The differentiation of (13) along the trajectory of (12) results in:

$$\begin{aligned}\dot{V} &= e\dot{e} + b\phi^T\begin{bmatrix}\gamma_1 & 0\\ 0 & \gamma_2\end{bmatrix}\dot{\phi} = \\ &= -a_m e^2 + be\phi^T\begin{bmatrix}\omega^*\\ \omega\end{bmatrix} - b\phi^T\begin{bmatrix}\gamma_1 & 0\\ 0 & \gamma_2\end{bmatrix}\begin{bmatrix}\dot{l}(t)\\ \dot{h}(t)\end{bmatrix}\end{aligned} \tag{14}$$

If are choosing for law adapting of the parameters for control law:

$$\begin{bmatrix}\dot{l}(t)\\ \dot{h}(t)\end{bmatrix} = \begin{bmatrix}\frac{1}{\gamma_1} & 0\\ 0 & \frac{1}{\gamma_2}\end{bmatrix}\begin{bmatrix}e\omega^* + l^* - l(t)\\ e\omega h^* - h(t)\end{bmatrix} \tag{15}$$

Then it can be obtained as follow:

$$\dot{V} = -a_m e^2 - be\phi^T\phi = -a_m e^2 - b\|\phi\|^2 \leq 0 \tag{16}$$

Therefore, according to the Lyapunov stability theorem, it can be concluded that the closed loop system is asymptotically stable.

III. Adaptive Control – Numerical Simulation

This section presents the results of the numerical simulation for the sensorless control of PMSMs with back-EMF sliding mode observer by using Simulink. Fig. 4 presents the block diagram for the Simulink implementation of the sensorless PMSM speed control system.

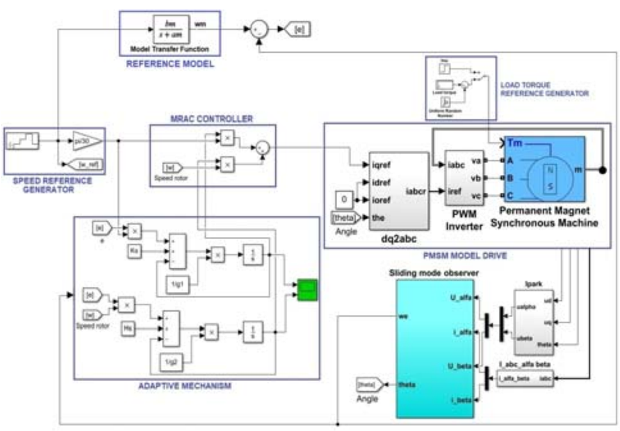

Fig. 3. MRAC control and back-EMF sliding mode observer - Simulink implementation.

The nominal parameters of PMSM are: the stator resistance R_s is 2.875Ω; q and d inductance L_q and L_d is 0.0085H; the combined inertia of rotor and load J is 0.8e-3kg·m^2; the combined viscous friction of rotor and load B is 0.005N·m·s/rad; the induced flux by the permanent magnets of the rotor in the stator phases ψ_f is 0.175Wb; and the pole pairs number P is 4.

The implementation in Simulink of the block diagram of the back-EMF sliding mode observer described above is presented in Fig. 3.

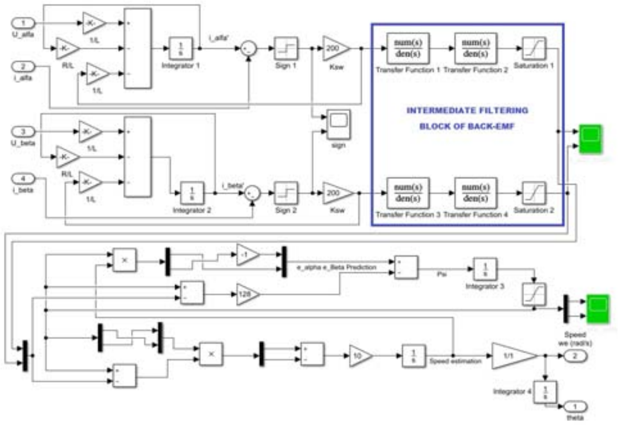

Fig. 4. Back-EMF and rotor speed sliding mode observer - Simulink implementation [21, 28, 30].

The main implemented blocks are highlighted: speed reference generator, MRAC controller, adaptive mechanism, model transfer function, load torque reference generator, PMSM model drive, and sliding mode observer.

Following the overall FOC-type control strategy, the results of the simulations where the speed controller in the outer control loop is PI-type or MRAC-type are presented comparatively, together with the adjustment mechanism of the control law parameters. The rotor speed and angle are provided by a back-EMF sliding mode observer. Regarding the transfer function of the reference model, a system of first order with aperiodic response, preferred in the electric drive control is selected.

If the PMSM has the nominal parameters presented at the beginning of this section, the PI-type control law given in equation (17) implemented in Simulink with adjustment parameters K_p=2 and K_i=50 (after practical tuning by using Ziegler-Nichols method), the speed reference is given by the next sequence: [0 0.25 0.5 0.75 1 1.25]s→[500 700 900 1100 700 500]rpm, the acceleration for speed ramps of ±1000rpm/s and, after 50ms from the start, the load torque reference is 0.1Nm, the numerical simulations results are shown in Fig. 5.

$$H_{PI}(s) = K_p + K_i\frac{1}{s} \tag{17}$$

In Fig. 6, for the same conditions regarding the nominal parameters of the PMSM, speed reference and load torque reference, such as the case where the speed controller is PI-type, the numerical simulations results are presented, but if the speed controller is MRAC-type, and the control law is given by equation (8), the adjustment law of the control law parameters is given by equation (15), and the reference model is a first-order type of transfer function with a time constant of 10ms.

It is noted that in the case of the PI controller, the only advantage relative to the MRAC-type controller is the rising time. In the case of the PI controller, it is noted that the peak values of the stator currents are three times higher than in the case of the MRAC controller (24A versus 8A). This observation is also valid for currents $I_{d,q}$ and for the electromagnetic torques. In terms of the settling time, the advantage of the PI controller disappears when there are load torque variations, as it will be further noticed.

If the nominal parameters vary (for example the value of the combined inertia of rotor and load increases by 50%, J=0.8e-3kg·m^2 becomes J=1.2e-3kg·m^2), the profile of the speed reference remains as in the presentation above, and the load torque reference is given by the next sequence: [0 0.05 0.8]s→[0.1 4 1]Nm, plus a uniform random sequence between -1Nm and 1Nm, the numerical simulation results for the PI controller are shown in Fig. 7, and the numerical simulation results for the MRAC controller are shown in Fig. 8.

In addition to the certain advantages of the MRAC controller compared to the PI controller, previously presented in the case of nominal parameters, it is noticed that in the case of the variation of nominal parameters and high variation of the load torque, the significant increase of the transient regime, and the occurrence of overshooting and errors in the stationary regime in the case of the PI-type controller are noticed in the details in Fig. 7. In terms of the implementation in embedded systems in real time, it is noticed that although the MRAC-type controller provides significantly superior results in proportion to the PI-type controller, the MRAC implementation additionally requires only the adjustment equations (15) which do not represent a significant burden of the DSP.

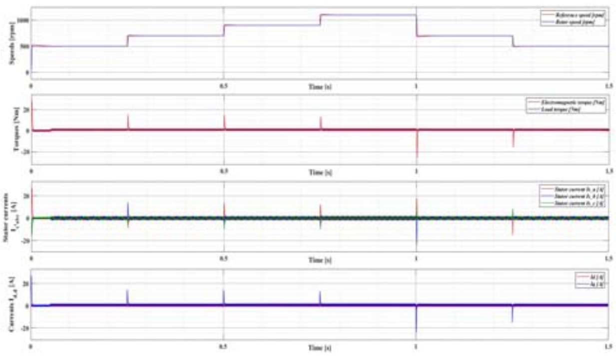

Fig. 5. Time evolution of the system with nominal parameters and PI controller.

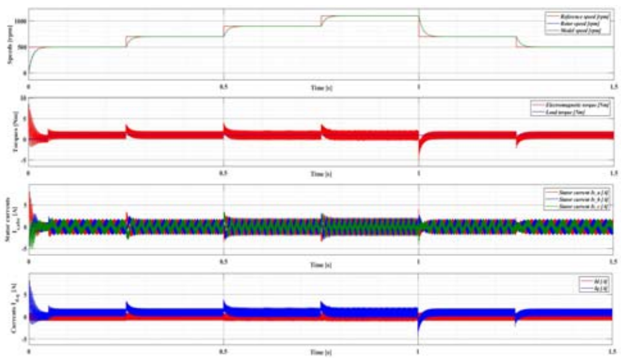

Fig. 6. Time evolution of the system with nominal parameters and MRAC controller.

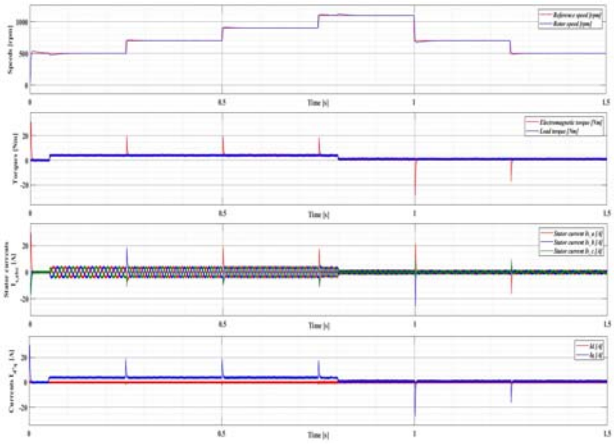

Fig. 7. Time evolution of the system with variation of J parameter and variable load torque and PI controller.

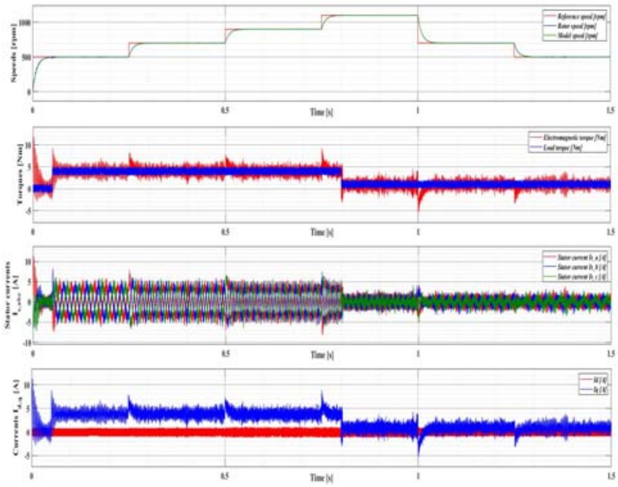

Fig. 8. Time evolution of the system with variation of J parameter and variable load torque and MRAC controller.

IV. Hybrid Model Of PMSM And Inverter

With the usual notations for a PMSM in d-q model on rotor reference frame, following [8, 9], the stator voltage equations can be written as:

$$\begin{aligned} v_q &= R_q i_q + \rho\lambda_d + \omega\lambda_d \\ v_d &= R_d i_d + \rho\lambda_d + \omega\lambda_q \end{aligned} \tag{18}$$

where R_q, R_d and L_q, L_d are the quadrature and direct axis winding resistances and inductances and ρ is the differential operator. The i_d, i_q and v_d, v_q are the d and q axes stator currents and voltages respectively. Mark the flux linkage as □ and the rotor angular velocity as ω. The flux linkages for q and d axes can be written as:

$$\begin{aligned} \lambda_q &= L_q i_q \\ \lambda_d &= L_d i_d + \phi \end{aligned} \tag{19}$$

For L_d=L_q=L and R_s=R_q=R, n_p is the number of pole pairs, J is the rotor inertia, K_t is the torque constant, B is the viscous friction coefficient, and T_L is the load torque, the reduced model presented in [9] is obtained in the following form:

$$\begin{pmatrix} \dot{i}_d \\ \dot{i}_q \\ \dot{\omega} \end{pmatrix} = \begin{pmatrix} -\frac{R_s}{L} & n_p\omega & 0 \\ -n_p\omega & -\frac{R_s}{L} & -\frac{n_p\phi}{L} \\ 0 & \frac{K_t}{J} & -\frac{B}{J} \end{pmatrix} \begin{pmatrix} i_d \\ i_q \\ \omega \end{pmatrix} + \begin{pmatrix} \frac{v_d}{L} \\ \frac{v_q}{L} \\ -\frac{T_L}{J} \end{pmatrix} \quad (20)$$

Following [16], Fig 9 presents in a simplified form the connection of a two-level, three-phase voltage inverter to a PMSM. Each inverter leg has two switching states, so there are eight possible switching states. These switching possibilities are presented in Table 1. These switching possibilities are indexed as j = 0...7, and will generate the corresponding inverter configurations.

TABLE I. SWITCHING STATE OF INVERTER LEGS

j	0	1	2	3	4	5	6	7
u_a	0	1	1	0	0	0	1	1
u_b	0	0	1	1	1	0	0	1
u_c	0	0	0	0	1	1	1	1

The hybrid model is presented next, where the voltage vector $[v_d(k)\ v_q(k)]^T$ can be expressed directly by using the inverter switching state vector, or by using the duty cycles of the switching state vector.

For a balanced load, the phase-to-neutral voltages can be expressed as functions of the half-bridge voltages (see Fig. 9).

$$\begin{bmatrix} v_{an}(k) \\ v_{bn}(k) \\ v_{cn}(k) \end{bmatrix} = \frac{1}{3} \cdot \begin{bmatrix} 2 & -1 & -1 \\ -1 & 2 & -1 \\ -1 & -1 & 2 \end{bmatrix} \cdot \begin{bmatrix} v_{a0}(k) \\ v_{b0}(k) \\ v_{c0}(k) \end{bmatrix} \quad (21)$$

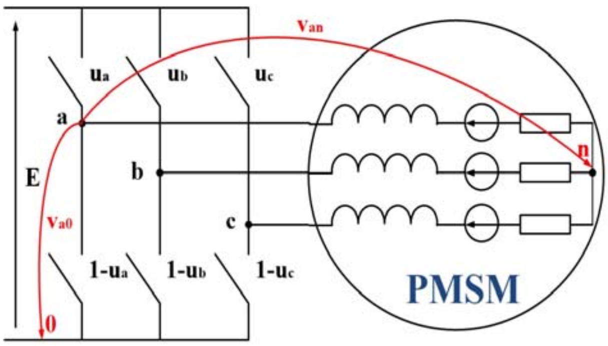

Fig. 9. Simplified representation of the system.

For $x \in \{a,b,c\}$, u_x represents the state of the leg x (if $u_x = 0$ then $v_{xo} = 0$; if $u_x = 1$ then $v_{xo} = E$, where E is the value of the voltage of the DC intermediate circuit). Based on this, it can be written as follows:

$$\begin{bmatrix} v_{an}(k) \\ v_{bn}(k) \\ v_{cn}(k) \end{bmatrix} = \frac{E}{3} \cdot \begin{bmatrix} 2 & -1 & -1 \\ -1 & 2 & -1 \\ -1 & -1 & 2 \end{bmatrix} \cdot \begin{bmatrix} v_a(k) \\ v_b(k) \\ v_c(k) \end{bmatrix} \quad (22)$$

The stator voltages in the α-β stator reference frame can be obtained from phase-to-neutral voltages:

$$\begin{bmatrix} v_\alpha(k) \\ v_\beta(k) \end{bmatrix} = \sqrt{\frac{2}{3}} \cdot \begin{bmatrix} 1 & -\frac{1}{2} & -\frac{1}{2} \\ 0 & \frac{\sqrt{3}}{2} & -\frac{\sqrt{3}}{2} \end{bmatrix} \cdot \begin{bmatrix} v_{an}(k) \\ v_{bn}(k) \\ v_{cn}(k) \end{bmatrix} \quad (23)$$

Following [2], the stator voltages in d-q frame can be obtained:

$$\begin{bmatrix} v_d(k) \\ v_q(k) \end{bmatrix} = E\sqrt{\frac{2}{3}} \cdot M(k) \cdot \begin{bmatrix} 1 & -\frac{1}{2} & -\frac{1}{2} \\ 0 & \frac{\sqrt{3}}{2} & -\frac{\sqrt{3}}{2} \end{bmatrix} \cdot \begin{bmatrix} u_a(k) \\ u_b(k) \\ u_c(k) \end{bmatrix} \quad (24)$$

$$= M(k) \cdot D \cdot u(k)$$

where $M(k) = \begin{bmatrix} \cos\theta(k) & \sin\theta(k) \\ -\sin\theta(k) & \cos\theta(k) \end{bmatrix}$, θ is the angular rotor position, D is a constant matrix and the leg state vector is $u(k) = [u_a(k) \quad u_b(k) \quad u_c(k)]$.

It is specified that the number of different configurations of the inverter is seven because the cases $u_a = u_b = u_c = 0$ and $u_a = u_b = u_c = 1$ lead to null voltages for PMSM.

To express the mean value of $v_{d,q}(k)$ (noted $\bar{v}_{d,q}(k)$), for a switching period T at step k, it is noted $\sigma_\lambda(k)$ the duty cycle of the leg λ ($\lambda \in \{a,b,c\}$). Based on these, the following relations are obtained:

$$\sigma_\lambda(k) = \frac{1}{T}\int_{kT}^{(k+1)T} u_\lambda(t)dt \quad (25)$$

$$\bar{v}_{d,q}(k) = \frac{1}{T}\int_{kT}^{(k+1)T} v_{d,q}(t)dt \quad (26)$$

For $\sigma(k) = [\sigma_a(k) \quad \sigma_b(k) \quad \sigma_c(k)]^T$, the duty cycle vector, equation (26) can be written as:

$$\begin{bmatrix} \bar{v}_d(k) \\ \bar{v}_q(k) \end{bmatrix} = M(k) \cdot D \cdot \sigma(k) \quad (27)$$

In the FOC control strategy (see Fig. 1) there is a cascade control system in which the outer loop is used to adjust the speed. The references for the internal current control loop are prescribed by the speed controller for I_q, and I_d is set to zero for torque maximization.

The hybrid equations (24) and (27) model the SVPWM (Space Vector Pulse Width Modulation) and the inverter with IGBT drivers blocks. Typically, the switching from one inverter configuration to another (see Table 1) is achieved in accordance with a switching table in the microcontroller's memory.

The next section presents a predictive control model with the current controllers from the FOC structure shown in Fig. 1, with a MPC type controller that will receive the reference from the speed controller and will command the IGBT drivers switching after a prediction of the I_d and I_q currents and minimization of an optimization criterion in order to obtain superior control performance.

V. PREDICTIVE CONTROL – MATHEMATICAL MODEL

This section presents the predictive control structure of currents for a PMSM where the global control structure is FOC type with a PI type external speed control that will generate a reference for the predictive controller, and the reference is chosen to maximize torque (I_d and I_q are stator currents in d-q axis frame). Due to the fact that the internal current controlling loop is much faster than the external speed control loop, it is assumed that the angular velocity ω is constant over the prediction horizon of the currents I_d and I_q.

Thus, the equation (20) describing the model of a PMSM can be written in a simplified form:

$$\begin{bmatrix} i_d(t) \\ i_q(t) \end{bmatrix} = \begin{bmatrix} -\frac{R}{L} & \omega(t) \\ -\omega(t) & -\frac{R}{L} \end{bmatrix} \cdot \begin{bmatrix} i_d(t) \\ i_q(t) \end{bmatrix} + \\ + \begin{bmatrix} \frac{1}{L} & 0 & 0 \\ 0 & \frac{1}{L} & \frac{\omega(t)}{L} \end{bmatrix} \cdot \begin{bmatrix} v_d(t) \\ v_q(t) \\ \phi \end{bmatrix} \quad (28)$$

It is assumed that the R, L and are constant, and the selected sampling period T is sufficiently low so that the displacement of the rotor between two successive sampling is negligible:

$$\begin{bmatrix} i_d(k+1) \\ i_q(k+1) \end{bmatrix} = A(k) \cdot \begin{bmatrix} i_d(k) \\ i_q(k) \end{bmatrix} + B \cdot \begin{bmatrix} v_d(k) \\ v_q(k) \end{bmatrix} + H(k) \quad (29)$$

where:

$$A(k) = \begin{bmatrix} 1-\frac{RT}{L} & T\omega(k) \\ -T\omega(k) & 1-\frac{RT}{L} \end{bmatrix}; B = \begin{bmatrix} \frac{T}{L} & 0 \\ 0 & \frac{T}{L} \end{bmatrix}; \\ H(k) = \begin{bmatrix} 0 \\ -\frac{T\omega(k)}{L}\phi \end{bmatrix} \quad (30)$$

For the general form of the discrete system (29) given by:

$$x_{k+i+1} = Ax_{k+i} + Bu_{k+i} + G\omega_k \quad (31)$$

$$y_{k+i} = Cx_{k+i} \quad (32)$$

where k is the present step to which the predictive controller is called, and i is the step in the prediction horizon N, the predictive control method implies constraints on the state and input variables and the minimization of a optimization criterion.

Constraints on the system may be written in general terms in the form of the equations below:

$$A_{u_{k+i}} u_{k+i} \le b_{u_{k+i}} \quad (33)$$

$$b^{lo}_{g(x_{k+i},u_{k+i})} \le g(x_{k+i}, u_{k+i}) \le b^{up}_{g(x_{k+i},u_{k+i})} \quad (34)$$

In the case of PMSM control, a series of constraints are required:

$$\begin{cases} v_d^2(t) + v_q^2(t) \le v_{\max}^2 \\ P_{PMSM}(t) \le P_{dc} \\ P_{PMSM}(t) = \frac{3}{2}\left(v_d(t) i_d(t) + v_q(t) i_q(t)\right) \\ I_{dc} \le I_{dc\max} \\ i_{d,q} \le i_{d,q\max} \end{cases} \quad (35)$$

where P_{dc} and I_{dc} are the power and current from intermediate DC circuit.

The optimization criterion in the general form can be written:

$$\min_{\substack{x_0,\dots,x_n \\ u_0,\dots,u_{N-1}}} J = \min_{\substack{x_0,\dots,x_n \\ u_0,\dots,u_{N-1}}} \left\| P_y (y_{k+N} - r_k) \right\|^2 \\ + \sum_{i=0}^{N} \left(\left\| Q_y (y_{k+i} - r_k) \right\|^2 + \left\| R_{\Delta u} u_{k+i} \right\|^2 \right) \quad (36)$$

where P, Q and R, are weighting matrices.

In the case of PMSM control due to the fact that the control loops are fast and the calculation time for the online implementation must be as low as possible, the optimization criterion can be chosen in one step by the minimization of the distance between the vector $X(k+1) = \left[i_d(k+1) \quad i_q(k+1) \right]^T$ and X* representing the references for Id and Iq provided by the speed controller. Thus (19) becomes:

$$J = \min_{1 \le i \le 7} \left| X_i(k+1) - X^* \right| \quad (37)$$

In order to obtain the PMSM model in which the inputs are the switching functions of the IGBT drivers $u(k) = \left[u_a(k) \quad u_b(k) \quad u_c(k) \right]$, is substitute equation (24) in (29), where vd and vq, are replaced by their mean values calculated for the switching period T in (26) , and the system is obtained in the next form:

$$X_i(k+1) = A(k) \cdot X_i(k) + B \cdot M(k) \cdot D \cdot u_i(k) + H(k) \quad (38)$$

where $X_i(k+1)$ is the state vector in which the system arrives after a sampling period in which the i configuration was applied (one of the seven possible inverter configurations according to Table 1).

At each sampling step, the stator currents, position and rotor speed are acquired to calculate the current vector X From the seven possible inverter configurations, the proper state vectors are derived from the equation (38) and the predictive algorithm selects the inverter configuration which, depending on the reference X^* will minimize the optimization criterion (37). This configuration will be applied to the inverter at the next sampling period. The predictive calculation algorithm works continuously, specifying that in order to minimize the number of commutations inside the inverter, if the minimization of the optimization criterion is provided by the free response of the system (given by classical SVPWM), then the configuration 0 in Table 1 is selected if the previous inverter configurations are 1, 3, or 5, otherwise configuration 7 is selected.

The block diagram of model predictive control is presented in Fig. 10:

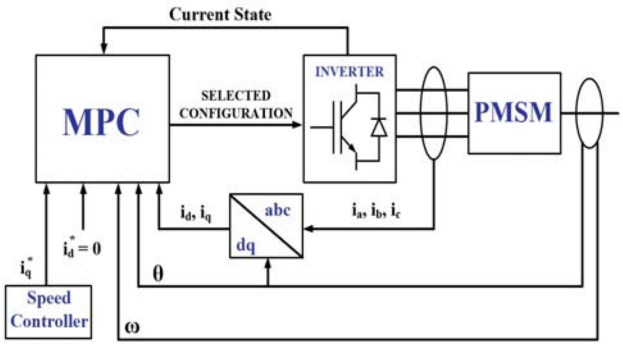

Fig. 10. Bloc diagram of MPC.

In the case of the sensorless control, the rotor speed will be provided by an observer. Due to the fact that the MPC algorithm is time consuming, it is necessary for the observer to be chosen so as not to significantly burden the DSP for implementation in an embedded system in real time. An observer involving a relatively small number of calculations is the MRAS observer according to [3, 18, 23].

The block diagram of MRAS is presented in Fig. 11. In case that even the PMSM is the reference model, I_d and I_q currents can be acquired directly. By using an adaptive model of the PMSM (see Fig. 12) described by an equation of the type (28) where the values of the I_d and I_q currents are updating according to ω, the intermediate signal ξ is formed:

$$\xi(t) = i_d \hat{i}_q - i_q \hat{i}_d - \frac{\phi}{L}(i_q - \hat{i}_q) \tag{39}$$

To assure the convergence of the observer in the adaptation mechanism (see Fig. 13) a PI controller is inserted. Based on these, the rotor speed is estimated by.

$$\hat{\omega}(t) = k_p \xi(t) + \int_0^t k_i \xi(\tau) d\tau \tag{40}$$

where k_p and k_i, are the adjustment parameters of the PI controller. The stability of the observer is proved using the Popov hyperstability theory according to [5].

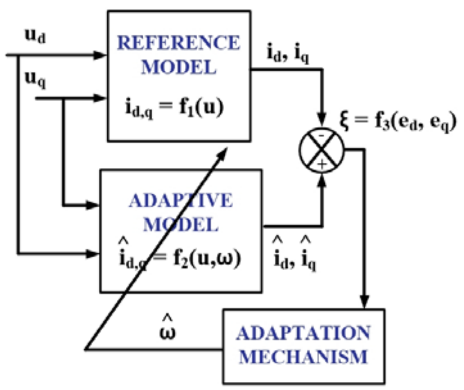

Fig. 11. Speed estimation scheme for MRAS.

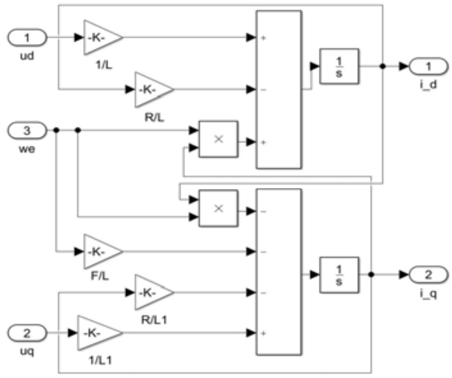

Fig. 12. Simulink block diagram of adaptive model.

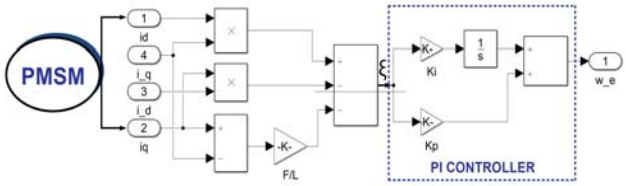

Fig. 13. Simulink block diagram implementation of adaptation mechanism.

VI. Sensorless Predictiv Control – Numerical Simulation

By using Matlab/Simulink, this section presents the results of the numerical simulation for the sensorless model of the predictive control of the PMSMs with MRAS observer. The nominal parameters of the PMSM used in simulation are presented in Section 3. Fig. 14 presents the block diagram for the implementation of this control structure in Simulink.

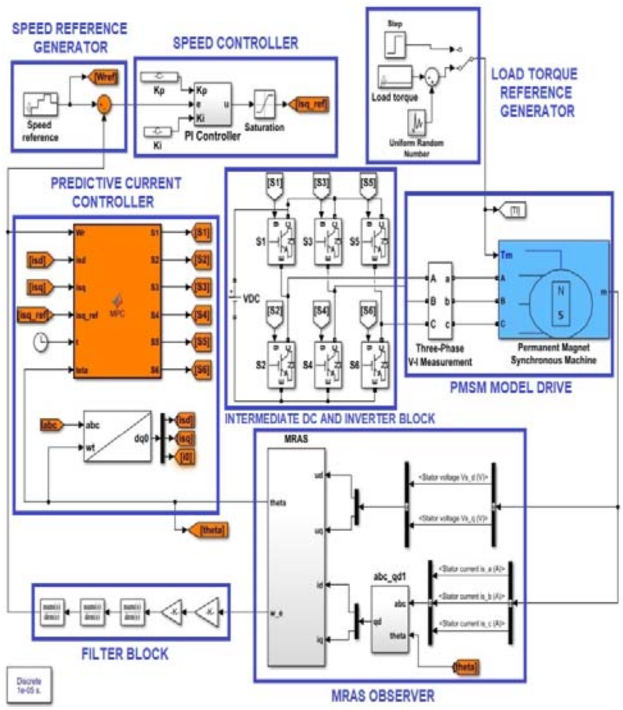

Fig. 14. Predictive current control and MRAS observer - Simulink implementation.

The main implemented blocks (see Fig. 14) of the control system are: speed reference generator, predictive current controller, intermediate DC and inverter block, filter block, PMSM model drive, load torque reference generator, and MRAS observer. Based on the FOC type global control strategy, the results of the numerical simulations in which the speed controller in the outer control loop remains the same, and the current controllers in the inner control loop from Fig. 1 (which are usually PI-type or on-off hysteresis controller) are replaced with a predictive current controller.

In case of sensorless control the speed and angle of the rotor are provided by a MRAS observer. Considering the nominal parameters of PMSM presented at the beginning of this section, for the speed controller, the control law is of the PI-type as in equation (17), implemented in Simulink with the adjustment parameters K_p=20 and K_i=200 (after practical tuning by using Ziegler- Nichols method), and current controllers are of the PI-type, with a suitable adjustment in order to obtain a more higher response velocity than the speed control loop.

Fig. 15 presents the numerical simulation results for the FOC strategy sensorless control and speed reference given by the next sequence: [0 0.25 0.5 0.75 1 1.25]s→[300 600 900 1100 800 500]rpm, and 50ms after the start, the load torque reference is 0.1Nm. For the same simulation conditions for the PMSM, the speed controller, and the same speed, acceleration, and torque reference values imposed above, Fig. 16 shows the results of the numerical simulations when the PI-type current controllers are replaced with a predictive current controller. Regarding the constraints of the type (37), the constraint is imposed for the reference current I_q, generated by the speed controller, not to exceed 10A. In the case of the PI-type current controllers, compared to the predictive current controller, there is a very small advantage regarding the response time by 6ms for PI-type controller versus the response time of 8ms for the predictive current controller.

In the case of the same profile of the speed reference presented above, but where the load torque reference is given by the next sequence: [0 0.05 0.8]s→[0.1 1 4]Nm, over which an uniform random sequence is added between -1Nm and 1Nm, and the combined inertia of the rotor and load increases by 50%, J=0.8e-3kg·m^2 become J=1.2e-3kg·m^2, the results of the numerical simulations for the PI-type current controllers are shown in Fig. 17, and for the predictive current controller, the numerical simulation results are presented in Fig. 18.

The occurrence of the overshooting and the significant increase of the settling time in the case of the current controllers and also a clearly superior quality response in the case of the predictive current controller can be noticed in case of a rapidly varying load torque and the variation of the nominal parameters. Also, it can be noticed that the maximum current values in the predictive current controller don't exceed 10A, and in the case of current controllers the maximum current values exceed 20A. Although the predictive current controller requires the selection of an optimal configuration and generally the predictive control is processing time consumer, in the system presented, by choosing a one-step prediction horizon and because the criterion optimization doesn't involve very complex arithmetic operations, it can be considered that the structure presented can be implemented in an embedded system in real time.

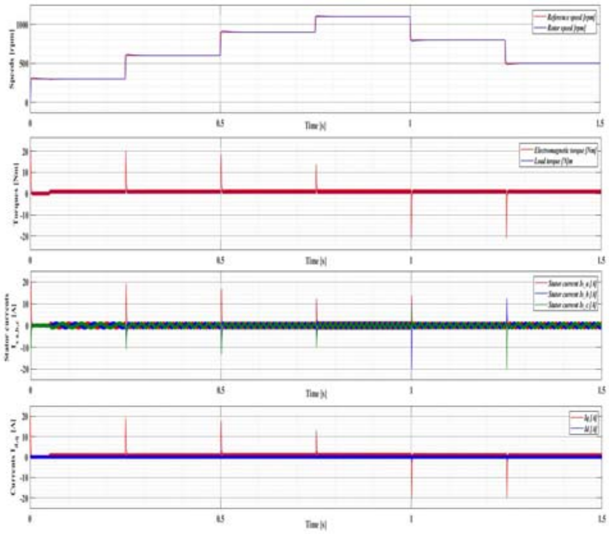

Fig. 15. Time evolution of the system with nominal parameters and PI controller.

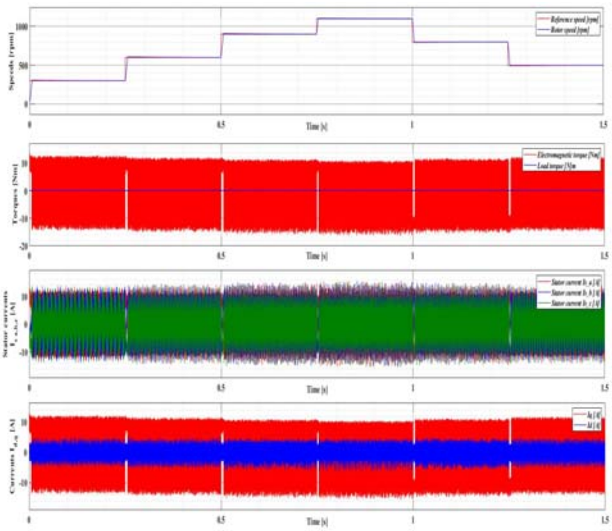

Fig. 16. Time evolution of the system with nominal parameters and MPC.

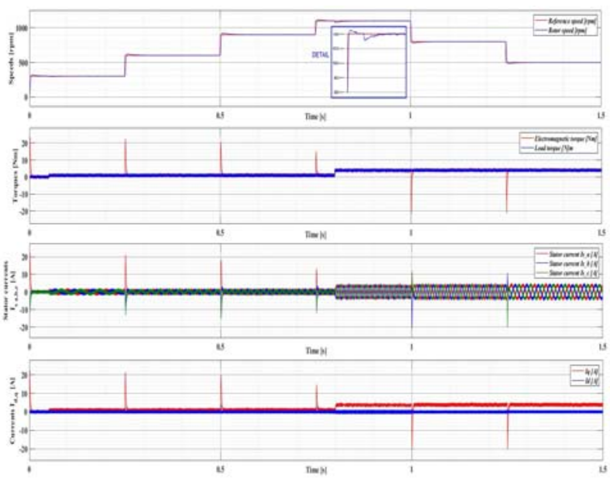

Fig. 17. Time evolution of the system with variation of J parameter and variable load torque and PI controller.

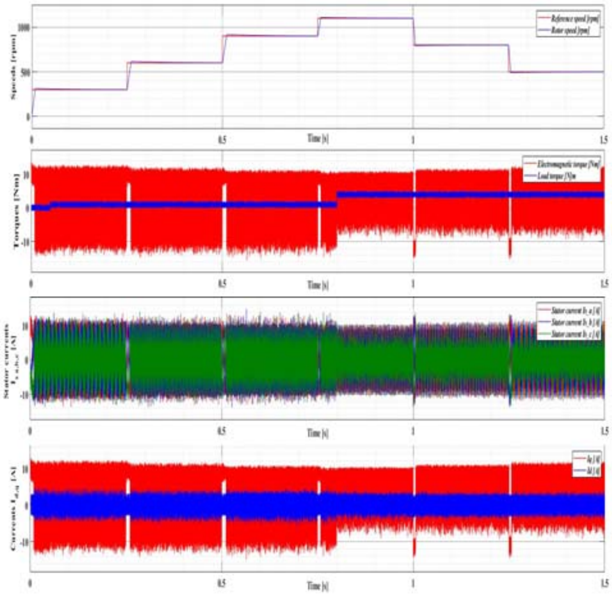

Fig. 18. Time evolution of the system with variation of J parameter and variable load torque and MPC.

VII. CONCLUSIONS

This article presents the implementation in Simulink of a FOC-type control structure for a PMSM, where the speed controller in the outer loop of the cascade control system is of MRAC type, and the speed is supplied by a back-EMF sliding mode observer.

The comparative results of the numerical simulations between the MRAC controller relative to the PI controller have been presented, where the nominal parameters vary, and the load torque has a very fast variation and a random component. It can be concluded that the adaptive control structure is considerably superior to the PI-type structure, and in terms of the implementation in real time in an embedded system, it introduces a small number of additional calculations, which makes it suitable for such an implementation in embedded systems in real time in future works.

It also, presents a sensorless MPC system for a PMSM in which the rotor speed is provided by a MRAS observer, in comparison to a standard FOC-type control structure.

The results of the numerical simulations show both the superiority of the MPC system, and the recommendation for the implementation in an embedded system in real time in future works, due to the relatively low complexity of the number of arithmetic operations required to implement the control algorithm and the speed estimation.

ACKNOWLEDGMENT

The paper was developed with funds from the Ministry of Research and Innovation as part of the NUCLEU Program: PN 19 38 01 03.

Contribution of authors:
Firs author – 60%
First coauthor – 40%

Received on October 2, 2019

Editorial Approval on November 15, 2019

REFERENCES

[1] N. Zhou, H. He, Z. Liu, and Z. Zhang, "UKF-based Sensor Fault Diagnosis of PMSM Drives in Electric Vehicles," *9th International Conference on Applied Energy (ICAE)*, Cardiff, UK, 2017, pp. 2276-2283.

[2] A. M. Saleque, A. M. A. Khan, S. H. Khan, E. Islam, and M. N. Chowdhury, "Variable speed PMSM drive with DC link voltage controller for light weight electric vehicle," *International Conference on Electrical, Computer and Communication Engineering (ECCE)*, Cox's Bazar, Bangladesh, 2017, pp. 145-151.

[3] L. Dhamo and A. Spahiu, "Simulation Based Analysis of Two Different Control Strategies for PMSM," International Journal of Engineering Trends and Technology, vol. 4, no. 4, pp. 596-602, April 2013.

[4] B. K. Bose, Modern power electronics and AC drives, Prentice Hall, Knoxville, Tennessee, USA, 2002.

[5] A. S. Mohamed, M. S. Zaky, A. S. Din, and H. Yasin, "Comparative Study of Sensorless Control Methods of PMSM Drives," in Innovative Systems Design and Engineering, vol. 2, no. 5, pp. 44-66, November 2011.

[6] A. Fezzani, S. Drid, A. Makouf, L. Chrifi-Alaoui, and M. Ouriagli, "Speed Sensoless Robust Control of Permanent Magnet Synchronous Motor Based on Second-Order Sliding-Mode Observer," in Serbian Journal of Electrical Engineering (SJEE), vol. 11, no. 3, pp. 419-433, October 2014.

[7] M. L. Mekha and G. Manju, "Speed Control of BLDC Motors Using MRAC," in International Research Journal of Engineering and Technology(IRJET), vol. 3, no. 6, pp. 2329-2334, June 2016.

[8] G. Feng and R. Lozano, Adaptive Control Systems, Newnes, MA, USA, 2009.

[9] X. Li and S. Li, "Speed Control for a PMSM Servo System Using Model Reference Adaptive Control and an Extended State Observer," in Journal of Power Electronics, vol. 14, no. 3, pp. 549-563, May 2014.

[10] M. Nicola and C. I. Nicola, "Sensorless Control for PMSM Using Model Reference Adaptive Control and back-EMF Sliding Mode Observer," *12th International Conference and Exhibition on Electromechanical and Energy Systems (SIELMEN)*, Chişinău, Moldova, 2019, pp. 317-322.

[11] X. Wu, H.Wang, X. Yuan, S. Huang, and D. Luo, " Design and Implementation of Recursive Model Predictive Control for Permanent Magnet Synchronous Motor Drives," in Mathematical Problems in Engineering, vol. 2015, pp. 1-10, April 2015.

[12] J. Rodriguez and P. Cortes, Predictive Control of Power Converters and Electrical Drives, John Wiley & Sons, Ltd, USA, 2012.

[13] L. Wang, S. Chai, D. Yoo, L. Gan, and K. Ng, PID and Predictive Control of electrical drives and power converters using Matlab/SIMULINK, John Wiley & Sons Ltd., Singapore, 2015.

[14] S. Ivanov, V. Ivanov,V. Rasvan, E. Bobasu, P. Popescu, and F. Stinga, "Predictive Versus Vector Control of the Induction Motor," *27th European Conference on Modelling and Simulation*, Alesund, Norway, 2013, pp. 434-440.

[15] T. Liu, H. S. Haslim, S. and Tseng, "Predictive speed-loop controller design for a synchronous reluctance drive system," *International Symposium on Fundamentals of Electrical Engineering*, Bucharest, Romania, 2016, pp. 1-6.

[16] F. Murel, X. Lin-Shi, J. Retif, B. Allard and C. Buttay, "A Comparative Study of Predictive Current Control Schemes for a Permanent-Magnet Synchronous Machine Drive," in IEEE Transactions on Industrial Electronics, vol. 56, no. 7, pp. 2715-2728, July 2009.

[17] M. Tang and S. Zhuang, "On Speed Control of a Permanent Magnet Synchronous Motor with Current Predictive Compensation," in Energies, vol. 12, no. 1, pp. 1-15, December 2018.

[18] M. Nicola and C. I. Nicola, "Sensorless Predictive Control for PMSM Using MRAS Observer," *12th International Conference and Exhibition on Electromechanical and Energy Systems (SIELMEN)*, Chisinau, Moldova, 2019, pp. 323-328.

[19] Y. Gao and Y. Gao, “Research of PMSM Fuzzy Direct Torque Control Based on Sliding Mode Observer,” *International Conference on Mechatronics and Automation (ICMA)*, Harbin, China, 2017, pp. 17-21.

[20] A. Mutlag, A. Mohamed, and H. Shareef, “A Nature-Inspired Optimization-Based Optimum Fuzzy Logic Photovoltaic Inverter Controller Utilizing an eZdsp F28335 Board,” in Energies, vol. 9, no. 3, pp. 1-32, March 2016.

[21] M. Nicola, C.I. Nicola, and M. Duță, “Adaptive Sensorless Control of PMSM using Back-EMF Sliding Mode Observer and Fuzzy Logic,” *The Electric Vehicles International Conference (EV)*, Bucharest, Romania, 2019, pp 1-6.

[22] A. Asri, M. N. Fazli, N. A. Salim, A. Omar, and M. Osman, “Speed Control Design of Permanent Magnet Synchronous Motor using Takagi-Sugeno Fuzzy Logic Control,” in Journal of Electrical Systems (JES), vol. 13, no. 4, pp. 689-695, November 2017.

[23] M. Nicola, D. Sacerdotianu, C. I. Nicola, and A. Hurezeanu, “Simulation and Implementation of Sensorless Control in Multi-Motors Electric Drives with High Dynamics,” in Advances in Science, Technology and Engineering Systems Journal (ASTEJ), vol. 2, no. 4, pp. 59-67, May 2017.

[24] J. Zambada and D. Deb, Sensorless Field Oriented Control of PMSM Motors – Aplication Note 1078, Microchip Technology Inc., 2010.

[25] V. Utkin, J. Guldner, J. Shi, Sliding mode control in electromechanical systems, second edition. Automation and Control Engineering, Taylor & Francis, 2009.

[26] L. I. Gliga, H. Chafouk, D. Popescu, and C. Lupu, “Comparison of State Estimators for a Permanent Magnet Synchronous Generator,” *22nd International Conference on System Theory, Control and Computing*, Sinaia, Romania, 2018, pp. 474-479.

[27] X. Liu, G. Zhang, L. Mei, and D. Wang, “Speed estimation and Parameters Identification simultaneously of PMSM based on MRAS,” in WSEAS Transactions on Systems and Control, vol. 12, no. 1, pp. 183-192, December 2017.

[28] M. Nicola, C. I. Nicola, and A. Vintilă, “Sensorless Control of Multi-Motors PMSM using Back-EMF Sliding Mode Observer,” *The Electric Vehicles International Conference (EV)*, Bucharest, Romania, 2019, pp 1-6.

[29] B. Liu, “ Speed control for permanent magnet synchronous motor based on an improved extended state observer,” in Advances in Mechanical Engineering, vol. 10, no. 1, pp. 1-12, January 2018.

[30] M. Nicola, C. I. Nicola, and D. Sacerdoțianu, “Sensorless Control of Multi-Motors BLDC using Back-EMF Observer,” *8th International Conference on Modern Power Systems (MPS)*, Cluj Napoca, Romania, 2019, pp. 1-6.